

Review

## Nanotribology of Symmetric and Asymmetric Liquid Lubricants

Shinji Yamada

Tokyo Research Laboratories, Kao Corporation, 2-1-3 Bunka, Sumida-ku, Tokyo 131-8501, Japan; Tel. +81 3 5630 9516; Fax: +81 3 5630 9330; E-Mail: yamada.s@kao.co.jp

Received: 15 December 2009; in revised form: 8 February 2010 / Accepted: 20 February 2010 /

Published: 15 March 2010

---

**Abstract:** When liquid molecules are confined in a narrow gap between smooth surfaces, their dynamic properties are completely different from those of the bulk. The molecular motions are highly restricted and the system exhibits *solid-like* responses when sheared slowly. This solidification behavior is very dependent on the molecular geometry (shape) of liquids because the solidification is induced by the packing of molecules into ordered structures in confinement. This paper reviews the measurements of confined structures and friction of symmetric and asymmetric liquid lubricants using the surface forces apparatus. The results show subtle and complex friction mechanisms at the molecular scale.

**Keywords:** nanotribology; friction; surface forces apparatus; confined liquids; lubricants; stick-slip; stiction; confinement-induced phase transitions

**Classification:** PACS 68.15.+e, 81.40.Pq

---

### 1. Introduction

Tribological properties of the molecularly thin films of a liquid lubricant confined between smooth surfaces are of importance in many academic research areas, as well as a great variety of practical applications. When the distance between the two surfaces (thickness of an intervening liquid film) is decreased to the order of a few molecular diameters, the molecular motions are highly restricted and the dynamic properties of the system cannot be understood simply by intuitive extrapolation of bulk rheological properties of the liquid [1-7]. This is an essential issue for developing and sustaining technologies such as the hard disk drives used for magnetic data storage and microelectromechanical systems (MEMS). In addition, the tribological properties of liquids in nanoscale confinement are also

important for the fundamental understanding of macroscopic or *realistic* tribology of liquid lubricated surfaces. Most of the practical or engineering surfaces are not molecularly smooth, but rough. The contact between the two surfaces occurs at protruding asperities where the intervening lubricant molecules are in nanoscale confinement. The nanotribology of liquid lubricants confined between smooth surfaces studied in this paper represents an ideal model for the sliding at a single asperity contact of rough surfaces.

There are two major experimental approaches to investigate the nanotribology of liquids in confinement: the surface forces apparatus (SFA) [1,8-10] and the atomic force microscope (AFM) [11]. The SFA measures the interaction between molecularly smooth mica surfaces (probe radius  $R \approx 1$  cm) separated by a thin liquid film. The true contact area, the local load and pressure, and the thickness of a sliding film are directly measured during sliding. The AFM measures normal and lateral (friction) forces between a sharp tip (tip radius  $R \approx 20$  nm) and a liquid lubricated surface in contact. The lubricant thickness and the true contact area are unknown in AFM friction measurements.

Due to the well-defined contact geometry and its potential to measure the contact area and the lubricant thickness accurately during sliding, the SFA is now commonly used to investigate the detailed friction mechanisms in confined liquid films. The contact geometry in the SFA is also suitable to compare the experimental results with computer simulations. Indeed, some important fundamental mechanisms of friction suggested by SFA experiments are directly supported by simulations [4,12,13].

In this paper, tribological properties of the molecularly thin films of liquid lubricants studied using the SFA are reviewed; considerable attention is focused on the effect of the geometry (shape) of lubricant molecules. Because the nanotribological properties of confined liquid lubricants are very dependent on the packing (ordering) of molecules between opposed surfaces, the geometry (shape) of molecules (symmetric or asymmetric) plays an essential role [1,14-20]. We start this paper by describing the force measurements using the SFA. Then, the liquid structures of symmetric and asymmetric liquids in confined geometries without sliding (static structures) will be examined. After that, the nanotribological properties (both static and kinetic friction) of confined liquid lubricants will be discussed in relation to their molecular geometries.

## 2. The Surface Forces Apparatus (SFA)

### 2.1. General feature of the SFA

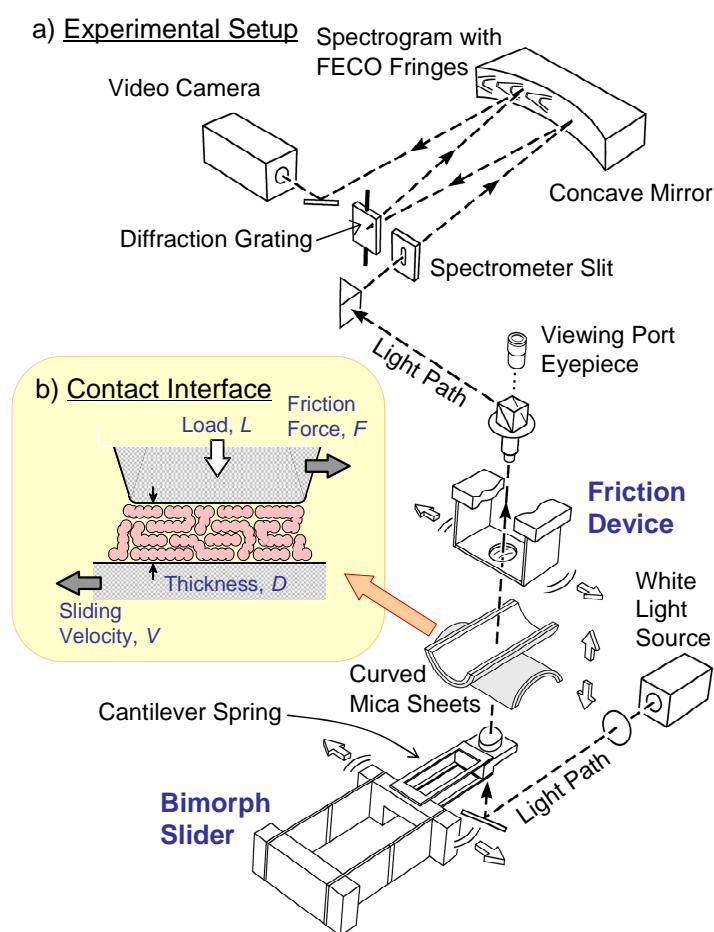
The surface forces apparatus (shown schematically in Figure 1 [21]) has become one of the standard tools for measuring forces between two smooth surfaces separated by liquids and vapors as a function of their separation [1,22]. By elastically compressing two initially curved surfaces, one can measure the forces (pressures) between two flat surfaces (this contact situation is the case for tribological measurement as described below). Molecularly smooth mica sheets are commonly used as the substrate surfaces.

The distance  $D$  between surfaces can be measured or controlled to better than 0.1 nm by the combination of different stage mechanisms such as micrometers, differential spring levers and a piezoelectric crystal transducer. The surface separation can be measured also to 0.1 nm using an optical “multiple beam interferometry” [23-25]. The fringes of equal chromatic order (FECO) are

obtained by passing a beam of white light through the substrate surfaces; the analysis of the fringe pattern enables us to measure the local radius  $R$ , flattened contact area  $A$ , thickness (surface separation)  $D$  and refractive index  $n$  of a confined liquid lubricant between surfaces.

For the normal force measurement between two mica surfaces, one of the surfaces is mounted at the end of a double cantilever spring. The deflection of this normal force measuring spring allows us to measure attractive and repulsive forces over the range of more than six orders of magnitude in force and from 0.1 nm to many microns in distance. Depending on the surface geometry, one can obtain the normal force  $F$  between two curved surfaces, or the pressure  $P (= F/A)$  between two flat surfaces.

**Figure 1.** Schematic drawing of the experimental set-up of the SFA friction measurements. The two surfaces are compressed together by applying normal load  $L$  (pressure  $P$ ). The intervening lubricant molecules are squeezed out from the contact interface and form a hard-wall film (inset). The bimorph slider is used to generate lateral motions of the lower surface at a constant sliding velocity  $V$  and the friction force  $F$  is measured by the deflection of the friction measuring spring that supports the upper surface. White light passing normally through the back-silvered mica sheets is focused on a spectrometer slit that results in the FECO interference fringe pattern. Detailed analysis of the fringes enables us to obtain the surface separation (thickness of intervening film  $D$ ) and the real contact area  $A$  during sliding. (Adapted with permission from [21]. Copyright 2000 by Elsevier.)



## 2.2. Tribological measurements

Lateral movement of the lower surface at a constant sliding velocity is accomplished with a piezoelectric “bimorph slider” by applying a triangular voltage to the bimorph strips [10]. Typical range of the sliding distance is about 50–100 $\mu\text{m}$ .

Lateral (friction) force is measured by the friction force measuring attachment called “friction device” [8,10]. The upper surface is supported by friction measuring springs of the friction device, and the lateral friction force is measured by the deflection of the friction springs which is detected by semiconductor strain gauges attached on the springs. Equipped with a bimorph slider and a friction device, one can measure friction force  $F$  at different applied loads  $L$  and sliding velocity  $V$ . The FECO fringes are always monitored during sliding, which enables us to obtain the film thickness  $D$  and the contact area  $A$  in real time. From the shape of the FECO, any wear or damage to the surface can be easily detected as soon as it occurs, allowing one to distinguish between undamaged sliding and friction with wear. All of the results included in this paper are obtained with atomically smooth mica surfaces (wearless friction).

## 3. Static Structures of Liquid Lubricant Films in Confinement

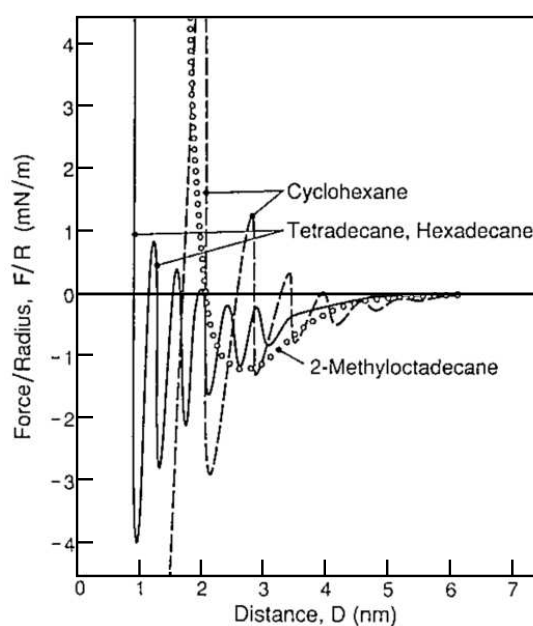
When the thickness of a liquid film between two smooth solid surfaces is decreased to the order of molecular dimensions, the system no longer behaves as a structureless continuum. The surface force between the two surfaces does not vary smoothly but oscillates with distance due to the contribution of *structural* or *solvation* forces [1]. The periodicity of the force oscillation corresponds to some mean size of the liquid molecules. Figure 2 shows the typical results of the structural forces of liquids measured using the SFA [1,26]. The examples of two different systems are shown: i) liquid molecules having symmetric shapes such as a spherical molecule (cyclohexane) and saturated linear-chain alkanes (tetradecane and hexadecane); and ii) asymmetric liquid molecules such as a branched alkane (2-methyloctadecane). Oscillatory structural force is observed for the symmetric systems; the periodicity corresponds to the diameter of the spherical cyclohexane and to the width of the hydrocarbon chain for the linear alkanes (the long axis of the hydrocarbon chain preferentially aligns parallel to surfaces). The force oscillation suggests that the molecules form discrete layer structures in the confined films. Asymmetric molecule 2-methyloctadecane exhibits a smooth and nonoscillatory force profile because the asymmetric shape of the molecule prevents it from packing into well-ordered discrete layers.

Spherical molecules, such as cyclohexane and octamethylcyclotetrasiloxane (OMCTS, not included in Figure 2), and linear hydrocarbon liquids, such as tetradecane and hexadecane, are the representative examples of symmetric liquid molecules. Both symmetric systems exhibit oscillatory structural forces in confinement as is shown in Figure 2, but the amplitude of the oscillation is larger for the spherical molecule (cyclohexane). Because spherical molecules do not have a major axis to orient to, the molecules can order into a structure not only in the direction normal to substrate surfaces (layering on surfaces) but also in the direction parallel to surfaces (positional ordering in the layered plain). On the other hand, for the linear chain molecules, they can form a discrete layer structure on surfaces but do not have a preferred orientation within the layered plane (no positional or in-plane ordering) [27]. As a

result, spherical molecules have more ordered structures than linear chain molecules, which results in the larger oscillation amplitudes in the force profile (spherical molecules obtain deeper free energy minima in the confined film).

The final film thickness under large applied load is important from the tribological viewpoint, which is evaluated from the normal force profiles (Figure 2). Compression of the two surfaces (decreasing the separation) squeezes out the intervening liquid molecules, but the molecules are not completely squeezed out from the interface and remain as a finite thickness film that supports the normal load (pressure). We can evaluate the final thickness by the distance where structural repulsive force diverges. This is called “hard-wall” thickness. Generally, symmetric liquid systems can pack into well-ordered structures and form thinner hard-wall films.

**Figure 2.** Forces between mica surfaces immersed in different liquid systems. Oscillatory force is observed for symmetric liquid systems (spherical molecule cyclohexane and linear chain molecules tetradecane/hexadecane), indicative of a discrete layer formation on surfaces. Asymmetric liquid (2-methyloctadecane) gives a smooth and continuous force profile. (Reproduced with permission from [26]. Copyright 1990 by American Institute of Physics).



## 4. Nanotribological Properties of Molecularly Confined Liquid Lubricants

### 4.1. General Features of the Friction and Lubrication of Confined Liquids

Figure 3 schematically shows the relationship between lateral friction or lubrication force and time for liquid lubricated surfaces [26]. When the thickness of the liquid film is thick enough to flow as a bulk Newtonian fluid (“thick film” in Figure 3a), lateral force rises with time after the commencement of sliding and reaches a plateau. This is the force  $F$  for the liquid to flow at a constant sliding velocity  $V$  and expressed as

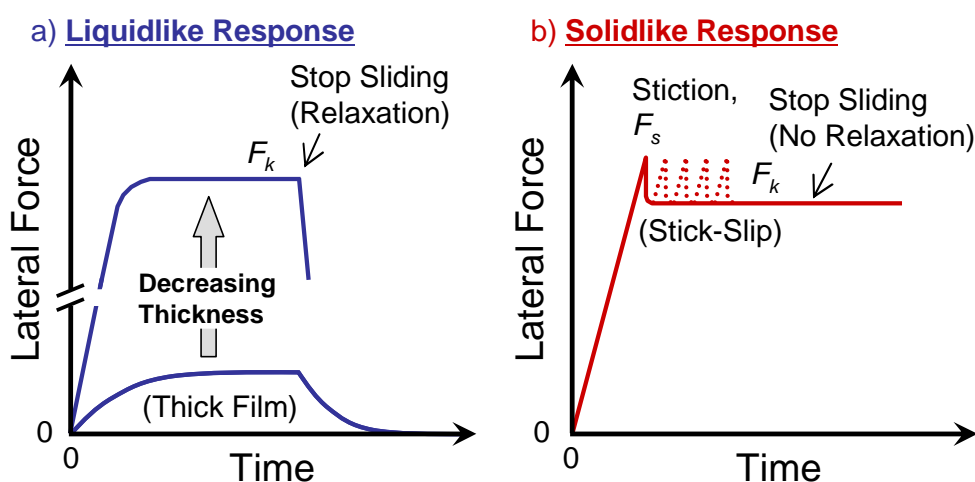
$$F = \eta A \dot{\gamma} \quad (1)$$

where  $\eta$  is the bulk viscosity,  $A$  is the surface area and  $\dot{\gamma}$  is the shear rate ( $= V/D$ ,  $D$  is the liquid film thickness). When sliding is stopped, the lateral force relaxes back to zero. When the thickness of the film is decreased to some molecular dimensions, the molecular motions are highly restricted and the viscosity of the system is increased by many orders of magnitude (referred to as effective viscosity  $\eta_{\text{eff}}$ ). The lateral force upon shearing is still described by Equation 1, but the force is much larger than that for the thick system.

For simple liquid systems, solid-like shear properties are often observed for their hard-wall state, which is shown in Figure 3b. The two surfaces are stuck to each other and move together at the commencement of sliding until the lateral force reaches a yield point ( $F_s$ , static friction force or stiction spike). After sliding occurs, the system sometimes exhibits stick-slip sliding at low shear rate (the lateral movement involves a repeated cycle of sticking and slipping). When sliding is stopped, the lateral force is stored and no force relaxation occurs.

Figure 3 represents the *ideal* examples for liquid-like and solid-like systems. The real friction force-time plots (friction traces) obtained from experiments exhibit mixed natures of liquid-like and solid-like behaviors, which will be discussed in the following sections.

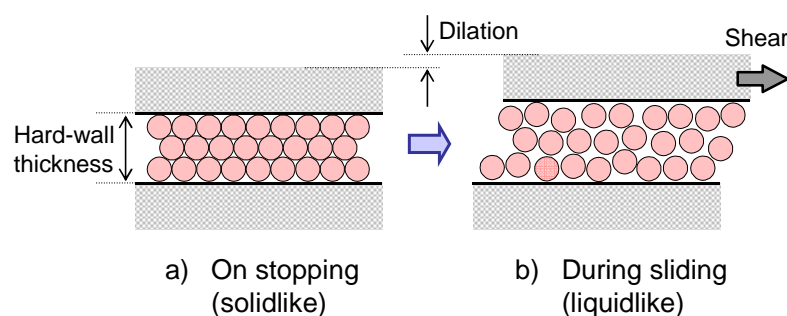
**Figure 3.** Two different lateral force responses between surfaces separated by liquid films. a) Liquid-like response. When the thickness of the liquid film is thick enough for the liquid to flow as a bulk Newtonian fluid, the lateral force-time profile shows typical liquid-like features. Nanoscale confinement increases the viscosity of the liquid; the lateral force increases by many orders of magnitude. b) For a well-ordered hard-wall film, solid-like shear response is observed, characterized by the static friction (stiction) and stick-slip sliding.



It is important to note that the thickness of a confined liquid film during sliding does not always equal its static hard-wall thickness, but varies. The typical example of the thickness change is schematically shown in Figure 4. In the static state, liquid molecules are geometrically confined and solidified (film is in a hard-wall state). In order to initiate sliding, lateral force must be applied that is large enough to *melt* the solid-like structure. This brings the density decrease of the system which is

achieved by the thickness increase (dilation) of the film, as is illustrated in Figure 4b. The order of the thickness change (dilation) is dependent on the molecular geometry, generally large for symmetric liquids and very small (sometimes below 0.1 nm [15,28,29]) for asymmetric liquids.

**Figure 4.** Shear-induced dilation of a confined liquid film. a) A liquid film is in a solid-like hard-wall state on stopping. Lateral sliding motion is initiated when applied shear force *melts* the solidified film. This is accompanied by the thickness increase (dilation) and density decrease as is shown in b).



#### 4.2. Static Friction (Stiction) of Confined Liquid Lubricants

We now describe the static friction (stiction) of confined liquid lubricants; it closely reflects the static liquid structure of the hard-wall films. In order to investigate the static friction behaviors of confined lubricants, SFA stop-start experiments were performed by a number of authors [14,15,18-20,30].

Figure 5 shows the example of a SFA stop-start experiment for the molecularly confined film of an asymmetric liquid lubricant, 1,3-dimethylbutyl octyl ether (DBOE) in the hard-wall thickness ( $D = 1.7$  nm) [18,20]. Figure 5a shows the exact friction traces obtained at different surface stopping times. Sliding is stopped for certain time  $t$ , then restarted; meanwhile the friction force is continuously measured as a function of time. If the stopping time is shorter than the characteristic nucleation time,  $\tau_n$ , there is no change in the friction when it is restarted. However, when the stopping time exceeds  $\tau_n$ , a stiction spike appears whose height  $\Delta F$  ( $= F_s - F_k$ ,  $F_s$  is a static friction force and  $F_k$  is a kinetic friction force) increases logarithmically with stopping time (Figure 5b). The  $\tau_n$  is obtained from the extrapolation of the logarithmic fit of the data to the abscissa. In the case of Figure 5a,  $\tau_n = 3.3$  s.

In general, there are two distinct aging mechanisms in stiction (static friction), geometrical aging and structural aging [31,32]. Geometrical aging affects the real contact area due to the plastic creep deformation of contact interfaces, and structural aging induces changes of the structure of intervening liquid films. Both aging mechanisms are time dependent; the contact area increases with aging time and the structural change of liquids also proceeds with time. In the SFA stiction measurements, the real contact area is always monitored and the result shown in Figure 5b is already in effect normalized by the contact area. Therefore, we can exclude the effect of geometrical aging and evaluate the effect of structural aging on stiction qualitatively and quantitatively. This is the big advantage to using SFA for the study of stiction behavior of confined liquid lubricants.

**Figure 5.** Stop-start measurements for the hard-wall film of an asymmetric liquid lubricant DBOE. a) Exact friction traces. When sliding is stopped, some molecular relaxation occurs and friction force initially decreases slightly. If the stopping time is shorter than the characteristic nucleation time,  $\tau_n$ , there is no measurable stiction spike, and when sliding is resumed it proceeds as if the surfaces have never been at rest. When stopping time is longer than  $\tau_n$ , a stiction spike is observed when sliding is resumed. The height of the spike increases with stopping time. In this figure,  $\tau_n \approx 3.3$ s. Experimental conditions: applied load  $L = 30$  mN (pressure  $P = 6.4$  MPa); sliding velocity  $V = 0.07$   $\mu\text{m/s}$ ; temperature  $T = 23$  °C. b) Effect of stopping time  $t$  on stiction spike height normalized by the contact area  $\Delta F/A$  for the DBOE films. Continuous logarithmic dependence of  $\Delta F/A$  on  $t$  is observed. [b) Reproduced with permission from [20]. Copyright 2009 by American Institute of Physics].

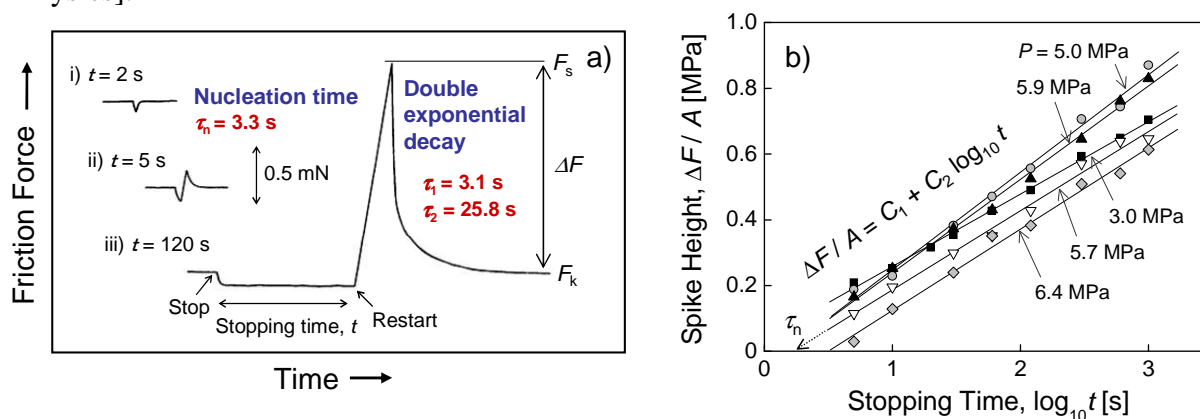
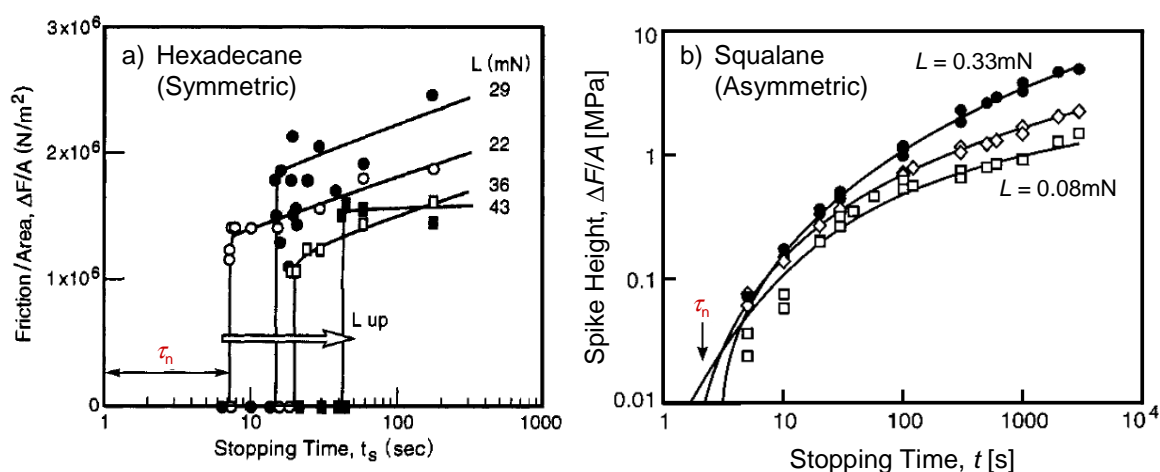


Figure 6 shows the other examples of the stiction spike measurements for symmetric (linear chain molecule hexadecane [14]) and asymmetric (squalane [15]) liquid systems. The results of the squalane system resemble those of DBOE; the spike height grows slowly and logarithmically with stopping time  $t$ . In contrast, symmetric liquid hexadecane displays a different behavior. An abrupt and finite stiction force appears once stopping time  $t$  is longer than  $\tau_n$  (Figure 6a). It is almost an “all or none” response, and only a slight increase in the spike height is observed for longer  $t$  ( $> \tau_n$ ).

The molecular mechanisms involved in the stop-start dynamics are discussed. In the SFA stop-start experiments, the confined film is slid before stopping and molecules in the film may not have a completely disordered structure but have shear-aligned configurations (discussed further in the following section) [15,26,33]. When sliding is stopped, the system relaxes from shear-aligned configuration to more disordered configuration. This molecular rearrangement induces a lateral force drop (relaxation) at stopping as is observed in Figure 5a. This rearrangement should be accompanied by a thickness decrease; Drummond and Israelachvili directly observed the thickness decrease at stopping for the confined squalane film [15]. If surface stopping time  $t$  is shorter than  $\tau_n$ , the film is in the disordered state (liquid-like) and does not have stiction spike at the commencement of sliding (liquid-like response as is shown in Figure 3a). In the disordered liquid-like film, molecular rearrangement continues with  $t$  and molecules tend to pack into *static* structure to obtain the free energy minima in confinement (like the schematic structure shown in Figure 4a); the film finally reaches a solid-like state. Hence, the nucleation time  $\tau_n$  is the time required for the conformational

(orientational) rearrangements of molecules from shear-ordered configuration to disordered *liquid-like* configuration and then to a static *solid-like* structure. The  $\tau_n$  is of course dependent on molecular mobility, and increasing applied load or decreasing temperature generally increases  $\tau_n$  because both effects decrease the molecular mobility in the film [14,18,20,30] (see Figure 6a). The brief mechanism discussed here is rather suitable to describe the behavior of asymmetric liquid molecules; symmetric liquids include some different features (discussed below).

**Figure 6.** Relationship between stiction spike height (normalized by the contact area)  $\Delta F/A$  and surface stopping time  $t$  for two different liquid systems; a) symmetric liquid hexadecane and b) asymmetric liquid squalane. The effects of  $t$  on the stiction spike height are different for the two systems (see text in detail). Experimental conditions: a)  $T = 21\text{ }^\circ\text{C}$ ,  $V = 0.17\text{ }\mu\text{m/s}$ ; b)  $T = 26\text{ }^\circ\text{C}$ ,  $V = 0.65\text{ }\mu\text{m/s}$ . [a) Adapted with permission from [14]. Copyright 1993 by American Chemical Society; b) Adapted with permission from [15]. Copyright 2000 by American Chemical Society.]



There are two possible solidification mechanisms of liquids in confinement; wall-induced epitaxial crystallization [16,34-36] and confinement-induced glasslike transitions [4,13,37-41]. This is a controversial issue and it is difficult to distinguish the two mechanisms precisely by SFA experiments. However, detailed analysis of the phase transition behaviors, particularly the continuous or abrupt features of the transitions, enables us to estimate the molecular mechanisms.

As was already mentioned, the stopping time dependence of the stiction spike height of the symmetric hexadecane shows an abrupt "all or none" behavior, which is reminiscent of a first-order-like transition. The first-order-like abrupt transition between liquid and solid-like phase for hexadecane is also observed for the transition between stick-slip and smooth sliding along with the change in the sliding velocity, which will be described in the next section.

In contrast, slow and continuous transition from liquid to solid-like state (continuous growth of  $\Delta F/A$  on  $t$ ) observed for the stiction behavior of asymmetric liquid systems, DBOE and squalane, resembles a glasslike transition. According to the conventional theories of glass transitions of bulk polymers, "slowing down" of molecular motions (increase in relaxation times) occurs due to the continuous decrease of collectively rearranging volume of molecules at low temperature [42]. It is reasonable to assume that the effect of confinement on the "slowing down" of molecular motions is

essentially equivalent to that of decreasing temperature [4,10,13,41-43]. Asymmetric molecules do not form discrete layer structures but pack more densely along with decreasing thickness, and the system should transit into glass at (or near) the hard-wall thickness.

Molecular mechanisms associated with the formation of stiction spike for asymmetric systems can be explained from the molecular volume decrease and continuous glasslike transition [20]. We consider that the critical nucleation time  $\tau_n$  is that required for the system to reach a critical molecular volume for a glasslike transition. When sliding is stopped, molecular rearrangement starts from shear-aligned kinetic structure to static structure as was mentioned. This rearrangement gradually reduces the molecular volume of molecules and a glasslike transition occurs at  $t = \tau_n$ . Glass has out of equilibrium structures and exhibits slow and continuous relaxation; the system is able to pack more densely and reach deeper energy minima along with  $t (> \tau_n)$ . Therefore, the shear stress required to bring the system out of the local energy minimum into a sliding configuration increases with time. This continuous increase commonly exhibits logarithmic dependence, which is observed in Figures 5b and 6b. Actually, this explanation is not limited to glasslike dynamics in confined liquids but generally applicable to the dynamics of bulk polymer glass [42,44-46].

We should note that the logarithmic dependence of static friction on surface stopping (aging) time is not a specific feature for nanotribological systems but observed in a variety of macroscopic friction systems and materials such as geological systems (earthquakes), polymer materials, papers, steels, *etc.* [31,32,47-50]. These macroscopic surfaces are not molecularly smooth but rough and the systems have multiple contacts at the sliding interface. For such cases, the origin of the logarithmic dependence of static friction on stopping time should be largely due to the contribution of geometric aging; the real contact area gradually and logarithmically increases with time because of the plastic creep deformation of the interface [31,49].

The force decay behavior of the stiction spike during slipping is also important. As is shown in Figure 5a, the force decay of the confined DBOE for the spike at  $t = 120$  s is fitted by a double exponential function and two relaxation times are obtained. In the case of Figure 5a, they are  $\tau_1 = 3.1$  s and  $\tau_2 = 25.8$  s, which are much longer than the time scales of any conceivable single molecule relaxations [51]. This indicates that the relaxation is governed by the cooperative molecular phenomena, which also implies glasslike dynamics for the DBOE system [20]. The double exponential fit of the force decay was also reported for the *stick-slip* friction of confined asymmetric squalane [16]; the relaxation times of  $\tau_1 = 1.7$  s and  $\tau_2 = 30.7$  s were obtained that are very close to the values for DBOE.

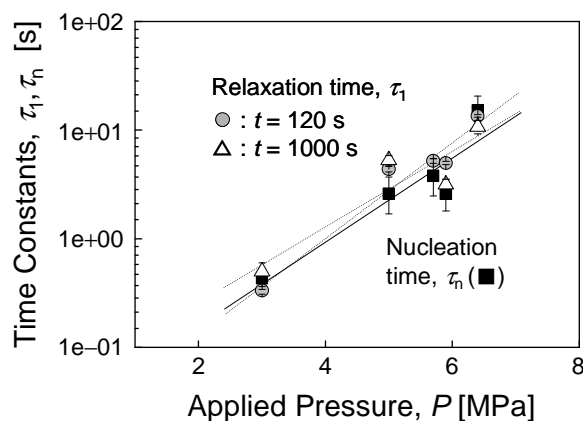
It is interesting to compare the molecular relaxation times on stopping and those on starting in the stop-start dynamics. For the DBOE system shown in Figure 5, the time scale for the phase transition from kinetic structure to solidlike structure on stopping is 3.3 s ( $= \tau_n$ ), which is very close to the short relaxation time of the stiction force decay on starting ( $\tau_1 = 3.1$  s). Figure 7 shows the comparison of the characteristic nucleation time  $\tau_n$  and the short relaxation time on starting  $\tau_1$  for the DBOE systems at different applied pressures. The two relaxation times are almost equal to each other at the same applied pressures, and both time constants exhibit exponential dependence on applied pressure [20]. The agreement of the two relaxation times implies that the solidification on stopping and its melting transition on starting are reversible molecular processes. According to the WLF (Williams-Landel-

Ferry) theories for the dynamics of bulk polymer glasses [42,52], the relationship between the relaxation time of molecular motion  $\tau$  and pressure  $P$  is given by

$$\ln \tau = \text{const.} + \frac{B}{f} = \text{const.} + BP \quad (2)$$

where  $B$  is a constant and  $f$  is the fractional free volume of molecules. Applicability of the WLF theories for the relaxation behavior of the confined asymmetric DBOE is another experimental evidence to support a glasslike mechanism of the solidification.

**Figure 7.** Effect of applied pressure on the molecular relaxation time on stopping  $\tau_n$  and that on starting  $\tau_1$  for the asymmetric liquid DBOE. The relaxation time  $\tau_1$  obtained at two different surface stopping times ( $t = 120$  and  $1000$  s) are plotted. Solid lines represent the exponential fit to the data using Equation 2. (Reproduced with permission from [20]. Copyright 2009 by American Institute of Physics.)



The agreement of  $\tau_n$  on stopping and  $\tau_1$  on starting is not observed for symmetric linear alkanes. As is shown in Figure 6a, the values of  $\tau_n$  for hexadecane are in the range of 7 to 30 s. On the other hand, the  $\tau_1$  values are much shorter than  $\tau_n$ . The  $\tau_1$  for hexadecane is too short to be evaluated precisely by a conventional SFA technique; lateral force dropped immediately to a kinetic friction force as soon as it reached a yield point [14]. This means that the solidification on stopping and its melting on starting for the symmetric hexadecane film are not the reversible molecular process. One of the plausible mechanisms of the dynamics is as follows [20]: the confined hexadecane film could be in a supercooled state when sliding is stopped, and the  $\tau_n$  may correspond to the time constant for the phase transition from supercooled state to crystalline along with aging. On the other hand, the  $\tau_1$  on slipping may reflect the melting transition of the crystal structure. It is difficult to clarify this speculation only by experiments; further studies including computer simulations are required to understand the molecular mechanisms underlying these dynamics.

#### 4.3. Kinetic Friction and Stick-Slip Sliding

According to the old theories of friction (Amontons' law [2,53]), friction force is independent of sliding velocity. This empirical friction law was established in 17th century based on the purely

geometrical model of interlocking asperities and is still effective for many practical tribological systems. However, for the friction of molecularly smooth surfaces separated by a confined liquid lubricant, we have to consider the effect of the mobility of confined liquid molecules instead of the effect of interlocking asperities. Therefore, we have to bring the idea of a “molecular relaxation (time scale)”, which is the main concept in rheology, also into tribology. Nanotribology of confined liquids must be discussed as a function of time (sliding velocity).

Figure 8 shows the schematic illustration of the effect of sliding velocity on friction force (“friction phase diagram” established by Yoshizawa and Israelachvili [2,14,54]). Friction force varies with sliding velocity and exhibits a maximum when the characteristic transit time (sliding velocity) equals the relaxation time of molecular motion at the sliding interface. The ratio between the two time scales is commonly known as the Deborah number,  $De$ , defined by

$$De = \text{relaxation time} / \text{transit time} \quad (3)$$

so that maximum friction occurs when  $De \approx 1$ . A single maximum peak is schematically illustrated in Figure 8. However, there are multiple molecular relaxation mechanisms at the sliding interface in real tribological systems and friction force-sliding velocity curves obtained from experiments suggest the existence of multiple peaks and valleys [18,19,30,55].

For a liquid or liquid-like film we expect the friction force to increase with the sliding velocity (like a Newtonian liquid) until the sliding velocity reaches  $De = 1$ , above which velocity the friction force falls. Stick-slip friction usually appears in the negative slope regime.

**Figure 8.** Schematic “friction phase diagram” showing the effects of sliding velocity on frictional energy dissipation [2,14,54]. Maximum friction occurs where  $De = 1$ . Increasing applied load (pressure) retards the molecular motions at the sliding interface and shifts the curve to lower sliding velocities. On the contrary, increasing temperature increases the molecular mobility and shifts the curve to higher velocities.

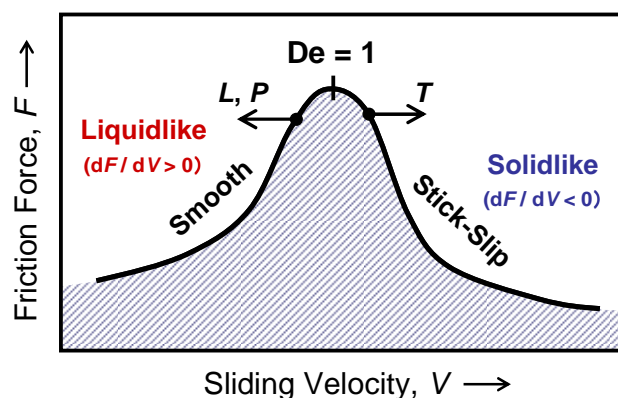


Figure 9 shows the relationship between shear stress  $S$  ( $=$  kinetic friction force  $F$  / contact area  $A$ ) and sliding velocity  $V$  for the asymmetric DBOE film [18]. Before we discuss the effect of sliding velocity, we briefly summarize the effect of applied load (pressure) on friction force (shear stress). The shear stress (friction force at unit area) increases with the increase of the applied pressure (applied load normalized by the contact area). According to the old theories of friction (Amontons’ law [2,53]), friction force  $F$  is proportional to applied load  $L$

$$F = \mu L \quad (4)$$

where  $\mu$  is the friction coefficient. This is an empirical law based on the purely geometrical model of interlocking asperities. Sliding of the two surfaces proceeds by overcoming the asperities (the upper surface moves up against the force of gravity to overcome the asperities, which gives a proportional load dependence). It is interesting to note that the friction of molecularly smooth surfaces also depends on applied load because the sliding is also accompanied by the lifting up of the upper surface by some fraction of an atomic or molecular dimension to overcome the molecular-scale asperities or surface lattices. In this situation, the normal load is enlarged by attractive surface forces and Amontons' law is modified by

$$F = F_0 + \mu L \quad (5)$$

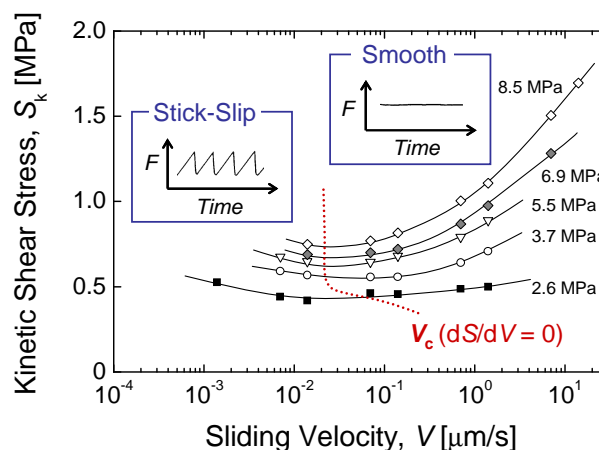
where  $F_0$  is the friction force at zero load [2]. For the friction of molecular smooth surfaces, finite friction force is occasionally observed even when the applied load is zero due to the contribution of adhesive surface forces, which is included as  $F_0$ . Note that according to Equation 5,  $\mu$  is given by the slope of the friction force vs. load curve,  $dF/dL$ , rather than the absolute value of  $F/L$ ; the latter is the more traditional definition of  $\mu$  given by Equation 4. Equation 5 appears to apply both at the macroscopic and nanoscopic scales (*scale invariant* friction law) [56]. In SFA friction measurements, the real contact area  $A$  can be directly measured by FECO and the magnitude of friction can be quantitatively described by the friction force at unit area, shear stress  $S$ . Then we obtain

$$S = \frac{F}{A} = \frac{F_0}{A} + \mu \frac{L}{A} = S_0 + \mu P \quad (6)$$

where  $S_0$  is the critical shear stress (shear stress at zero normal pressure) [2]. If the surface force between two surfaces separated by a lubricant liquid is purely repulsive,  $F_0 \approx 0$  ( $S_0 \approx 0$ ) and friction force is simply proportional to  $L$  (Equation 4, load-controlled friction). On the other hand, for highly adhesive systems,  $F_0$  ( $S_0$ ) is large and  $\mu$  is very small (adhesion-controlled friction). The friction of molecularly smooth mica surfaces covered by a surfactant monolayer sometimes shows typical adhesion-controlled friction ( $S = S_0$  and  $\mu \approx 0$ ) [57]. The friction coefficients  $\mu$  ( $= dF/dL$ ) of the DBOE system in Figure 9 range from 0.01 to about 0.2 depending on the sliding conditions (e.g., sliding velocity and applied pressure). Symmetric liquid systems generally give larger  $\mu$ , sometimes larger than 1 [2,14,26]. For a detailed discussion on the effects of loads or pressures, see Reference [2] for example.

Now we discuss the effect of sliding velocity on friction in Figure 9. The shear stress curves for the DBOE show apparent sliding velocity dependence. At low sliding velocity ( $V < 0.1 \mu\text{m/s}$ ), shear stress decreases with  $V$ . Shear stress curves exhibit a minimum at  $V \approx 0.02 \mu\text{m/s}$  and above the velocity shear stress increases with  $V$ . This velocity dependence implies that there are at least two friction force maxima ( $De = 1$ ) associated with two different molecular relaxation processes at low  $V$  and high  $V$  regions, which are outside the sliding velocity range covered by the measurement. Friction features dramatically change with sliding velocity. The system shows stick-slip friction in the negative slope regime ( $dS/dV < 0$ ) and smooth sliding is observed for the positive slope regime ( $dS/dV > 0$ ) (see the insets of Figure 9). The velocity for the friction minimum ( $dS/dV = 0$ ) corresponds to the critical velocity ( $V_c$ ) for the stick-slip friction.

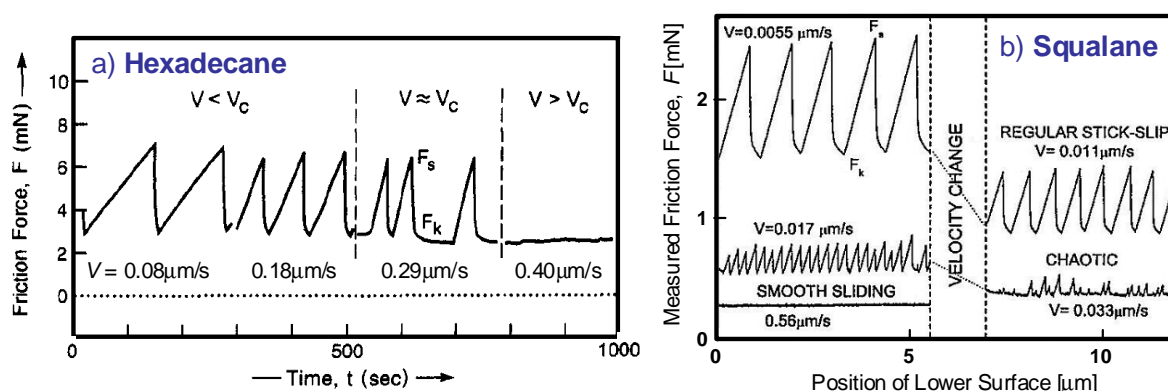
**Figure 9.** Relationship between shear stress and sliding velocity for the confined asymmetric films of DBOE at different applied pressures. Friction curves have a shallow minimum at the sliding velocity of about  $0.02 \mu\text{m/s}$  where stick-slip to smooth sliding transition occurs. The friction traces in insets show the typical examples of the traces below and above the critical velocity  $V_c$ . (Adapted with permission from [18]. Copyright 2005 by American Chemical Society.)



Stick-slip friction is observed for many different confined liquid systems, both symmetric and asymmetric molecules, sheared at low sliding velocity. Figure 10 shows the examples of the stick-slip friction of a) symmetric hexadecane [14,58] and b) asymmetric squalane [16,59]. For the symmetric hexadecane, the stick-slip amplitude does not depend much on sliding velocity when sliding velocity is lower than the critical stick-slip velocity  $V_c$ . At  $V = V_c$ , stick-slip spikes eventually disappear and smooth sliding is observed. On the other hand, the stick-slip behavior of the confined squalane is apparently continuous; stick-slip amplitudes gradually and continuously decrease with increasing sliding velocity and the system shifts to smooth sliding when sliding velocity reaches  $V_c$ .

There are three theoretical models for the fundamental mechanisms of stick-slip friction; rough surfaces model, velocity-dependent friction model, and phase transition model [2,14,60]. For the confined lubricant liquid systems studied here, the phase transition model is the most important mechanism to understand the stick-slip behavior. In this model, cyclic transitions occur between static state (solidlike phase during sticking) and kinetic state (liquid-like phase during slipping). Therefore, it is reasonable to correlate the molecular mechanisms of stick-slip dynamics with those of stiction dynamics discussed in the previous section.

**Figure 10.** Comparison of the stick-slip behaviors between a) symmetric liquid hexadecane and b) asymmetric squalane. The effects of sliding velocity on the stick-slip behaviors are different; the transition from stick-slip to smooth sliding at  $V_c$  is abrupt (discontinuous) for hexadecane and is continuous for squalane. Experimental conditions: a)  $T = 18\text{ }^\circ\text{C}$ ,  $V_c \approx 0.4\text{ }\mu\text{m/s}$ , dry  $\text{N}_2$  gas (relative humidity = 0%); b)  $T = 26\text{ }^\circ\text{C}$ . In this experiment, it is difficult to precisely determine  $V_c$  because it is difficult to distinguish chaotic regime and smooth regime. [a) Adapted with permission from [14]. Copyright 1993 by American Chemical Society.; b) Adapted with permission from [16]. Copyright 2001 by the American Physical Society.]



Stick-slip friction is obtained at a constant *driving* velocity. However, the *relative* velocity between the two surfaces is not constant but varies during the stick-slip cycles. During sticking, the *relative* velocity between surfaces is zero and the two sticking surfaces move at a given *driving* velocity [61]. Decreasing driving velocity prolongs the time in the sticking regime, which corresponds to the long stopping (aging) time in the stop-start stiction measurements. In contrast, stick-slip does not appear at high driving velocity because the system does not have enough time to solidify, which corresponds to the case of no stiction spikes at  $t < \tau_n$  in the stop-start measurements. On the basis of this idea, critical sliding velocity for the stick-slip friction  $V_c$  and the critical nucleation time  $\tau_n$  for stiction is quantitatively correlated as follows [2,14]:

$$V_c = \frac{(F_s - F_k)}{5K\tau_n} \quad (7)$$

where  $(F_s - F_k)$  is the stick-slip amplitude and  $K$  is the spring constant of the friction measuring spring. This equation does not consider the sliding velocity dependence of stick-slip amplitude and therefore could be rather suitable for the abrupt (discontinuous) transition systems. Indeed the critical velocity for the symmetric hexadecane is well predicted by Equation 7 inserting the values obtained from sliding and stop-start measurements.

#### 4.4. Comparison of the Molecular Mechanisms between Stiction and Stick-Slip Friction

It is interesting to compare the shear dynamics between stiction and stick-slip friction because both include solid-liquid transitions in confinement and under shear. The solidification mechanism (first-

order-like or glasslike) that governs the dynamics of stiction and stick-slip friction is basically the same for most of the symmetric and asymmetric liquids in confinement. However, for the case of asymmetric DBOE, stiction and stick-slip friction are governed by different solidification mechanisms, which will be described below.

For the symmetric hexadecane film, stick-slip amplitude is not very sensitive to sliding velocity ( $V < V_c$ ), and the transition from stick-slip to smooth sliding occurs abruptly at  $V_c$  (Figure 10a). This “all or none” feature is similar to that we observe for the stiction dynamics of the same system (Figure 6a). No stiction spike appears when the stopping time  $t < \tau_n$ . When  $t$  exceeds  $\tau_n$ , spike appears whose height does not depend much on  $t$ . These results lead to a conclusion that a first-order-like solidification (crystallization) should be the major mechanism for the stick-slip and stiction dynamics of symmetric hexadecane in confinement [2,14,16,35-36,62,63]. This explanation is consistent with the well-ordered layer structure in the hexadecane film as probed by a normal force measurement (Figure 2). Spherical molecules such as cyclohexane and OMCTS also show abrupt (discontinuous) solid-liquid transitions in stick-slip and stiction dynamics.

The stick-slip to smooth transition for the asymmetric squalane exhibits a continuous nature (Figure 10b). Stick-slip amplitude is large at low sliding velocity and gradually decreases with the increase of sliding velocity, and stick-slip disappears at  $V_c$  (stick-slip amplitude diminishes below the noise level). This smooth transition reminds us of a continuous solidification behavior in the stiction dynamics of the same systems. As was already discussed, the stiction dynamics of asymmetric squalane are successfully explained from the theories of a confinement-induced glasslike transition [4,13,16,38-41]. The same mechanism can be applied to the stick-slip dynamics; increase in the stick-slip amplitude along with the decrease in sliding velocity could result from the more densely-packed structures induced by long time aging (low sliding velocity gives long sticking or aging time in the stick-slip cycles). This structural change also induces the growth of the length scales of correlated structures in three dimensions. Drummond and Israelachvili [15] reported that branched hydrocarbon lubricants such as poly- $\alpha$ -olefin and a mixture of branched hydrocarbons also exhibit a continuous glasslike nature of the dynamics in stick-slip and stiction behaviors.

Strictly speaking, the stopping (aging) conditions are not exactly the same between during sticking in the stick-slip cycles and during stopping in stiction. As was already mentioned, in the stiction measurements, lateral force drops immediately when lateral movement is stopped (Figure 5a), indicative of some molecular rearrangements from kinetic structures (possibly have shear-aligned conformations) to static structures (more disordered conformations). On the other hand, in the stick-slip cycles the two sticking surfaces move together at a given *driving* velocity and lateral force is continuously applied (no relaxation in the lateral stress), which may have the effect of maintaining the shear-aligned kinetic conformations even during sticking. The different force relaxation behaviors in stiction and stick-slip friction do not have an essential effect on the dynamics of symmetric and asymmetric systems, but have a significant effect on the dynamics of the confined DBOE system.

Yamada [18,20] compared the stiction and stick-slip friction of asymmetric liquid DBOE in confinement. Continuous stiction spike behavior against stopping time is observed as is shown in Figure 5b. Logarithmic dependence of the spike height on stopping time suggests glasslike dynamics. In addition, the relaxation time analysis (Figure 7) also implies the glasslike solidification nature. Figure 11 shows the stick-slip amplitude of the same system as a function of sliding velocity. The

stick-slip amplitude does not decrease continuously with the increase of sliding velocity but the stick-slip abruptly disappears near  $V_c$ , which resembles a first-order-like transition. The stick-slip amplitude does not depend much on applied pressure, which is also consistent with the first-order-like mechanism (glasslike dynamics are more sensitive to applied pressure [42,52]). The different solidification mechanisms in stiction and stick-slip dynamics for the confined DBOE film could be explained as follows: i) aging with lateral stress relaxation (in the case of stiction) leads to a “rather disordered” glasslike structure, and ii) aging without lateral stress relaxation (in stick-slip friction) may retain the shear-aligned molecular conformations even during sticking [33] which could lead to a crystal-like structure. Israelachvili *et al.* [64] studied the shear dynamics of an anisotropic (dye) molecule using the FECO spectroscopy in the SFA and concluded that lateral shear force actually leads to a local alignment of molecules and triggers nucleation and crystallization. The same effect could be expected for the stick-slip dynamics of the DBOE system.

**Figure 11.** Stick-slip amplitudes as a function of sliding velocity for the hard-wall films of DBOE at different applied pressures. The inset shows the typical stick-slip shapes obtained at  $P = 4.7$  MPa.  $T = 23$  °C. (Adapted with permission from [20]. Copyright 2009 by American Institute of Physics.)

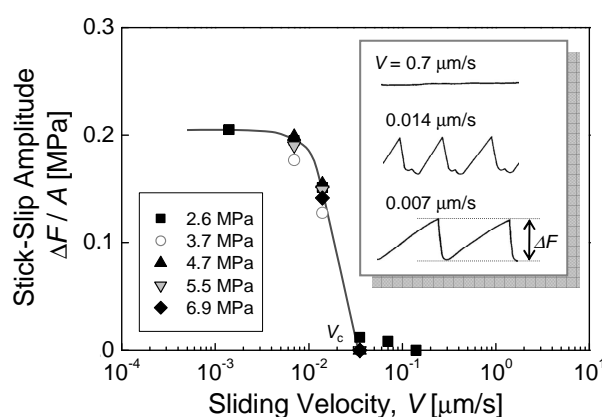


Table 1 summarizes the stiction and stick-slip dynamics of symmetric and asymmetric liquid systems in confinement [20]. Symmetric spherical and linear chain molecules exhibit discontinuous stiction and stick-slip dynamics, indicative of a first-order-like crystallization in the static-kinetic transitions. In contrast, (highly-) asymmetric liquid molecules such as squalane tend to exhibit a continuous nature of stiction and stick-slip transitions on the basis of a glasslike transition. For the continuous glasslike systems, the stiction spike height and stick-slip amplitude reach plateaus at long stopping or sticking time. This is possibly due to the fact that the length scales of cooperative rearrangement (essential nature of a glasslike transition) become saturated in a confined geometry [20]. Table 1 includes an exceptional example (asymmetric DBOE) that exhibits different solidification mechanisms between stiction and stick-slip friction, which may reflect the effect of lateral (residual) stress during stopping (aging) and resulting conformational relaxations.

**Table 1.** Comparison of the stiction and stick-slip behaviors for symmetric and asymmetric liquid systems in confinement [20].

		symmetric (e.g., hexadecane [14,58])	asymmetric (e.g., DBOE [18,20])	highly asymmetric (e.g., squalane [16,59])
stiction behavior	spike height vs. stopping time	immediately increase to its plateau when $t$ exceeds $\tau_n$ (“all or none” behavior)	increase logarithmically with $t$ , long time required to reach to a plateau	
	possible mechanism	“discontinuous” first-order-like transition (crystallization)	“continuous” glasslike transition	
stick-slip behavior	stick-slip amplitude vs. sliding velocity	insensitive to $V$ ( $V < V_c$ ), stick-slip abruptly disappears at $V_c$ (“all or none” behavior)		gradually decrease with $V$ , shift to smooth regime at $V_c$
	possible mechanism	“discontinuous” first-order-like transition (crystallization)		“continuous” glasslike transition

#### 4.5. Complex Shear Behaviors of Confined Asymmetric Liquids

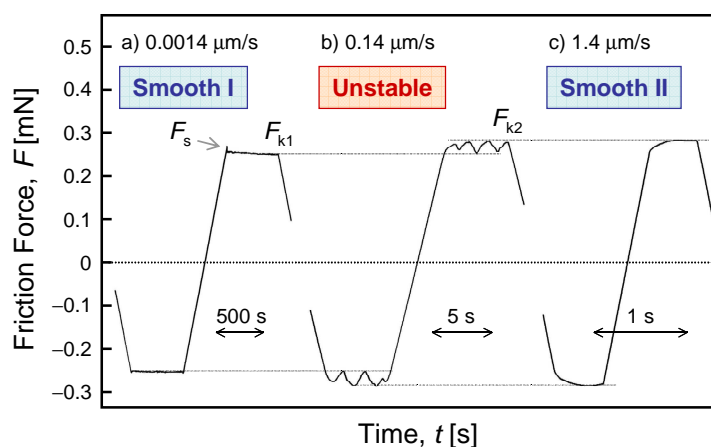
Because asymmetric liquid molecules form disordered structures in confinement, their dynamic properties are much more complex than those of symmetric liquids. In this section, we describe some examples of the complex shear behaviors of asymmetric liquids.

Figure 12 shows the friction traces for the confined films of an asymmetric liquid lubricant 1,3-dimethylbutyl hexadecyl ether (DBHE) in the hard-wall state (thickness  $D = 1.7\text{nm}$ ) [19]. Friction traces at three different sliding velocities are shown. At low sliding velocity (a), smooth sliding is observed (Smooth I regime). Static friction force ( $F_s$ ) appears at the commencement of sliding. At high sliding velocity (c), smooth sliding is again observed (Smooth II regime). In this regime, the system exhibits no static friction. Between the two smooth regime, unstable sliding is observed; friction force exhibits cyclic “bumps and valleys”. Most of the unstable sliding such as stick-slip friction appears *below* some critical sliding velocity (below a smooth sliding regime). However, for the DBHE system there are (at least) two critical velocities and two smooth regimes; the unstable regime locates *between* the two smooth regimes.

The unique velocity dependence of the friction behavior, two smooth sliding regimes at low and high sliding velocity and unstable regime between them, was first reported by Drummond *et.al.* [65,66] for the sliding of surfactant monolayer-coated mica surfaces in water. They measured the sliding velocity dependence of friction behavior in a very wide velocity range and found a stick-slip regime between two smooth sliding regimes. The stick-slip behavior is very different from common stick-slip friction; stick-slip spikes pointed *down* rather than up (“inverted” stick-slip friction). The molecular mechanism of the new unstable sliding was studied experimentally [67] and theoretically

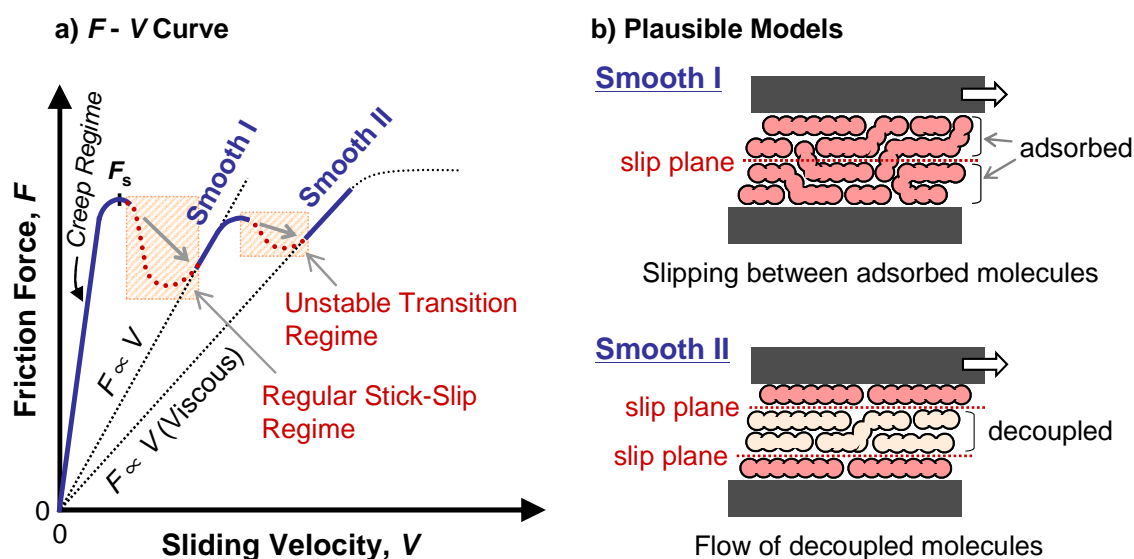
[68], and the following model has been proposed. The smooth sliding at low sliding velocity is governed by the formation and rupture of adhesive bonds between shearing surfaces (elastic contribution), which is accomplished by the slipping between adsorbed surfactant molecules. The smooth sliding at high sliding velocity is governed by the flow of molecules under shear (viscous contribution), which implies the desorption of surfactant molecules from substrate surfaces. The “inverted” stick-slip friction is the transition state between the two different kinetic sliding states, slipping between adsorbed molecules and flow of detached molecules.

**Figure 12.** Friction traces for the hard-wall film of DBHE at three different sliding velocities. Three different friction regimes are observed. a) Smooth I regime at low sliding velocity. After a change in the driving direction, static friction is observed. b) Unstable regime. The friction force exhibits cyclic bumps and valleys. c) Smooth II regime. Smooth sliding is again observed. No static response is observed after the change in the driving direction. (Adapted with permission from [19]. Copyright 2008 by American Chemical Society.)



On the basis of the above models, Yamada [19] proposed plausible mechanisms to explain the unstable sliding of DBHE (Figure 13b). The DBHE molecule has an asymmetric shape and the confined film has rather a disordered structure. The molecules in the film should interdigitate between each other. At low sliding velocity, molecules in the film are adsorbed on highly-adhesive mica surfaces and slipping could occur between the adsorbed molecules (Smooth I regime). Increasing sliding velocity tends to stretch or “iron” the molecules, which reduce the interdigitation of molecules between each other [15,69,70]. Then, molecules at the center of the film may be decoupled from mica surfaces and flow with sliding motions (Smooth II regime). Figure 13a schematically shows the friction map for the confined DBHE system; showing the different friction states depending on the sliding velocity. At very low sliding velocity, regular stick-slip sliding (transition between static friction and kinetic friction) is expected, which is deduced from the existence of the static friction response in Figure 12a and stop-start stiction measurements [19].

**Figure 13.** a) Schematic friction map (friction force-sliding velocity curve) for the confined DBHE film. The stop-start measurement for this system shows a stiction spike after a long stopping time. Therefore, friction maximum at very low sliding velocity is expected, which corresponds to a static friction force. b) The plausible molecular models for the two smooth sliding regimes are shown, which represent the effect of sliding velocity on the change of molecular conformations and resulting shift of slip planes. (Adapted with permission from [19]. Copyright 2008 by American Chemical Society.)



We should add two more points on the complexity of the nanotribology of asymmetric systems. First, the friction mechanisms of confined asymmetric liquids include a glasslike long-range cooperative effect, which gives longer correlation times for relaxation and also *longer sliding distances* to reach a steady sliding state [15,16]. Second, chaotic stick-slip behavior is occasionally observed just below  $V_c$  (Figure 10b) [15,16,59,71], which is also a characteristic feature of the complex tribology of asymmetric liquid systems. The transition from stick-slip to smooth sliding along with the sliding velocity is continuous for glasslike systems, and the definition of  $V_c$  is the velocity above which no more stick-slip spikes are observed (stick-slip amplitude is below the noise level). Near  $V_c$ , static force necessary to initiate sliding of surfaces becomes extremely sensitive to sliding conditions such as perturbation, fluctuation or sliding velocity; this is the reason for the chaotic stick-slip friction.

#### 4.6. Future Prospects

In this paper, nanotribological properties of the molecularly confined films of symmetric and asymmetric liquid lubricants investigated using the SFA are reviewed. Many aspects of liquid structures and resulting nanotribological dynamics are successfully explained from the view of two solidification mechanisms of liquids in confinement and under shear; first-order-like discontinuous transition (crystallization) and continuous glasslike transitions. However, we have to mention that there are still controversial discussions on the solidification mechanisms in confined films:

- i) It is difficult to exclude the possibility of the formation of poly-crystalline states for asymmetric liquid systems; we cannot precisely distinguish the two states (poly-crystalline or glasslike) by conventional SFA experiments.
- ii) There are publications that report *continuous* glasslike dynamics for highly-symmetric spherical liquid molecules. Granick *et al.* examined the nanorheological properties of the molecularly thin films of OMCTS using the SFA and found the continuous increase of relaxation times along with the thickness decrease [38,72]. This is totally incompatible with the abrupt dynamic transitions between solid-like state and liquid-like state for symmetric liquid systems described in this paper. The apparatus and experimental conditions of Granick's works are slightly different from those of most of the works referred in this paper, but we do not have sufficient explanations for the discrepancy.
- iii) Bureau [73] recently reported that the liquid structures in confinement are very dependent on the confinement rate. They studied the molecular layering of a linear alkane n-hexadecane and found that the layering (ordering) is observed when the liquid is confined at an extremely low confinement rate. Increasing confinement rate induces disordered liquid structures even for the symmetric linear liquid. The results included in this paper were obtained under sufficiently low confinement rate; detailed analysis of the rate effect should further improve our understanding on the structuring of liquids in confinement.
- iv) The structures and properties in confined liquid films are not uniform in both thickness and in-plane directions. Density distribution of molecules is not uniform in the thickness direction as probed by normal force measurements (see Figure 2) [1]. Also, the contact pressure for Hertzian contact shows a maximum at the center of the contact area, which induces non-uniform molecular density distributions within the contact area [74]. Friction behavior observed by the SFA represents the *average* properties of the entire film and masks a variety of different local mechanisms of sliding within the film.

Improvement of the experimental technique with the SFA could shed new light on the complex behaviors of the dynamics of confined liquids. Heuberger *et al.* improved the SFA by introducing fast spectral correlation (FSC) interferometry [6,75]. The accuracy of the thickness and refractive index measurements of confined liquids using this technique is improved by a factor of about 10 to 30 compare with the conventional setting of the SFA measurements. Kurihara *et al.* established a new shear force measuring technique called shear force resonance method [76,77]. The advantage of this method is an extremely high sensitivity to any change in the fluidity of intervening liquid films attained by the high shear resonance response. Also, combination of the SFA with a variety of spectroscopic techniques is proposed recently, which enables us to investigate the detailed and/or local structures of confined liquids during shear. Israelachvili *et al.* studied the structure and dynamics of the molecularly confined films of a liquid-crystal using the combination of SFA and X-ray scattering [78]. Granick and coworkers have reported the measurements of confined liquid dynamics using the SFA with two spectroscopic techniques; fluorescence correlation spectroscopy [74,79], and confocal Raman spectroscopy [80-82]. These studies reveal the heterogeneous dynamics of liquid molecules within the confined films.

## 5. Summary and Conclusions

The shear properties of liquid lubricants confined at nanoscale are very different from those of bulk rheological properties. The relaxation times of molecular motions are prolonged by many orders of magnitude and the systems show solid-like responses when sheared slowly. The solidification of liquids in confinement and resulting dynamic properties are very dependent on the geometric feature (shape) of liquid molecules because the dynamics are governed by the packing of molecules in confined geometries and during shear. Detailed friction measurements of the molecularly thin films of symmetric and asymmetric liquid lubricants using the surface forces apparatus enable us to discuss the relationship between molecular geometry and nanotribological properties.

Symmetric liquid molecules, such as linear chain molecules and spherical molecules, tend to pack into well-ordered structures in confinement. The stiction and stick-slip friction behaviors suggest a first-order-like discontinuous transition between solid-like phase and liquid-like phase upon shearing, indicative of a confinement-induced and/or shear-induced crystallization. In contrast, stiction and stick-slip properties of liquids having asymmetric molecular shapes generally exhibit a continuous nature of the solid-liquid transitions, indicative of a glasslike transition induced by confinement and shear. The nanotribological dynamics of asymmetric liquid molecules are much complex due to a variety of packing structures in confinement and during shear.

## Acknowledgements

The author is grateful to J. Israelachvili for enlightening discussions and permission to use Figure 1, to M. Nagayama-McCrum for editing the manuscript, and to Kao Corporation for permission to publish this paper.

## References and Notes

1. Israelachvili, J.N. *Intermolecular and Surface Forces*, 2<sup>nd</sup> Ed.; Academic Press: London, UK, 1991.
2. Israelachvili, J.; Berman, A.D. Surface Forces and Microrheology of molecularly thin liquid films. In *CRC Handbook of Micro/Nanotribology*, 2<sup>nd</sup> Ed.; Bhushan, B., Ed.; CRC Press: Boca Raton, FL, USA, 1999; Chapter 9, p. 371.
3. Granick, S. Motions and Relaxations of Confined Liquids. *Science* **1991**, *253*, 1374-1379.
4. Robbins, M.O.; Muser, M.H. Computer Simulations of Friction, Lubrication and Wear. In *Modern Tribology Handbook*, Volume One; Bhushan, B., Ed.; CRC Press: Boca Raton, FL, USA, 2001; Chapter 20, p. 717.
5. Klein, J.; Kumacheva, E. Confinement-Induced Phase Transitions in Simple Liquids. *Science* **1995**, *269*, 816-819.
6. Heuberger, M.; Zach, M.; Spencer, N.D. Density Fluctuations under Confinement: When is a Fluid Not a Fluid? *Science* **2001**, *292*, 905-908.
7. Yamada, S. Layering Transitions and Tribology of Molecularly Thin Films of Poly(dimethylsiloxane). *Langmuir* **2003**, *19*, 7399-7405.

8. Israelachvili, J.; McGuiggan, P.M.; Homola, A.M. Dynamic Properties of Molecularly Thin Liquid Films. *Science* **1988**, *240*, 189-191.
9. van Alsten, J.; Granick, S. Molecular Tribometry of Ultrathin Liquid Films. *Phys. Rev. Lett.* **1988**, *61*, 2570-2573.
10. Luengo, G.; Schmitt, F.J.; Hill, R.; Israelachvili, J. Thin Film Rheology and Tribology of Confined Polymer Melts: Contrast with Bulk Properties. *Macromolecules* **1997**, *30*, 2482-2494.
11. Bhushan, B. Boundary Lubrication Studies Using Atomic Force/Friction Force Microscopy. In *CRC Handbook of Micro/Nanotribology*, 2<sup>nd</sup> Ed.; Bhushan, B., Ed.; CRC Press: Boca Raton, FL, USA, 1999; Chapter 8, p. 357.
12. Bhushan, B.; Israelachvili, J.N.; Landman, U. Nanotribology: Friction, Wear and Lubrication at the Atomic Scale. *Nature* **1995**, *374*, 607-616.
13. Robbins, M.O.; Baljon, A.R.C. Response of Thin Oligomer Films to Steady and Transient Shear. In *Microstructure and Microtribology of Polymer Surfaces*; American Chemical Society: Washington, DC, USA, 2000; Chapter 6, p. 91.
14. Yoshizawa, H.; Israelachvili, J. Fundamental Mechanisms of Interfacial Friction. 2. Stick-Slip Friction of Spherical and Chain Molecules. *J. Phys. Chem.* **1993**, *97*, 11300-11313.
15. Drummond, C.; Israelachvili, J. Dynamic Behavior of Confined Branched Hydrocarbon Lubricant Fluids under Shear. *Macromolecules* **2000**, *33*, 4910-4920.
16. Drummond, C.; Israelachvili, J. Dynamic Phase Transitions in Confined Lubricant Fluids under Shear. *Phys. Rev. E* **2001**, *63*, 041506.
17. Gourdon, D.; Israelachvili, J. Transitions between Smooth and Complex Stick-Slip Sliding of Surfaces. *Phys. Rev. E* **2003**, *68*, 021602.
18. Yamada, S. Nanotribology of Ethers: Effects of Molecular Asymmetry and Fluoroalkyl Chains. *Langmuir* **2005**, *21*, 8724-8732.
19. Yamada, S. Dynamic Transitions in Molecularly Thin Liquid Films under Frictional Sliding. *Langmuir* **2008**, *24*, 1469-1475.
20. Yamada, S. Structural Aging and Stiction Dynamics in Confined Liquid Films. *J. Chem. Phys.* **2009**, *131*, 184708.
21. Golan, Y.; Drummond, C.; Israelachvili, J.; Tenne, R. *In Situ* Imaging of Shearing Contacts in the Surface Forces Apparatus. *Wear* **2000**, *245*, 190-195.
22. Israelachvili, J.; McGuiggan, P.M. Adhesion and Short-Range Forces between Surfaces. Part I: New Apparatus for Surface Force Measurements. *J. Mater. Res.* **1990**, *5*, 2223-2231.
23. Israelachvili, J. Thin Film Studies Using Multiple-Beam Interferometry. *J. Colloid Interface Sci.* **1973**, *44*, 259-272.
24. Heuberger, M.; Luengo, G.; Israelachvili, J. Topographic Information from Multiple Beam Interferometry in the Surface Forces Apparatus. *Langmuir* **1997**, *13*, 3839-3848.
25. Tadmor, R.; Chen, N.; Israelachvili, J.N. Thickness and Refractive Index Measurements Using Multiple Beam Interference Fringes (FECO). *J. Colloid Interface Sci.* **2003**, *264*, 548-553.
26. Gee, M.L.; McGuiggan, P.M.; Israelachvili, J.N. Liquid to Solidlike Transitions of Molecularly Thin Films under Shear. *J. Chem. Phys.* **1990**, *93*, 1895-1906.
27. In-plane ordering of molecules is affected by the surface structure of substrate material. The mica surface used as the standard substrate for SFA experiments has a crystalline (periodic) lattice,

which induces the ordering of molecular axis [1]. This effect results in the local alignment of molecules, but there is no preferred orientation within the whole contact area.

28. Dhinojwala, A.; Bae, S.C.; Granick, S. Shear-Induced Dilation of Confined Liquid Films. *Tribol. Lett.* **2000**, *9*, 55-62.
29. Demirel, A.L.; Granick, S. Lubricated Friction and Volume Dilatancy are Coupled. *J. Chem. Phys.* **2002**, *117*, 7745-7750.
30. Yamada, S.; Israelachvili, J. Friction and Adhesion Hysteresis of Fluorocarbon Surfactant Monolayer-Coated Surfaces Measured with the Surface Forces Apparatus. *J. Phys. Chem. B* **1998**, *102*, 234-244.
31. Caroli, C. Baumberger, T.; Bureau, L. Static Aging vs. Dynamic Rejuvenation in Solid Friction. *J. Phys. IV France* **2002**, *12*, Pr9-269-273.
32. Bureau, L.; Baumberger, T.; Caroli, C. Rheological Aging and Rejuvenation in Solid Friction Contacts. *Eur. Phys. J. E* **2002**, *8*, 331-337.
33. Drummond, C.; Alcantar, N.; Israelachvili, J. Shear Alignment of Confined Hydrocarbon Liquid Films. *Phys. Rev. E* **2002**, *66*, 011705.
34. Thompson, P.A.; Grest, G.S.; Robbins, M.O. Phase Transitions and Universal Dynamics in Confined Films. *Phys. Rev. Lett.* **1992**, *68*, 3448-3451.
35. Thompson, P.A.; Robbins, M.O.; Grest, G.S. Structure and Shear Response in Nanometer-Thick Films. *Israel J. Chem.* **1995**, *35*, 93-106.
36. Rabin, Y.; Hersht, I. Thin Liquid Layers in Shear: Non-Newtonian Effects. *Physica A* **1993**, *200*, 708-712.
37. Hu, H.W.; Carson, G.A.; Granick, S. Relaxation Time of Confined Liquids under Shear. *Phys. Rev. Lett.* **1991**, *66*, 2758-2761.
38. Demirel, A.L.; Granick, S. Glasslike Transition of a Confined Simple Fluid. *Phys. Rev. Lett.* **1996**, *77*, 2261-2264.
39. Granick, S. Soft Matter in a Tight Spot. *Phys. Today* **1999**, *52*, 26-31.
40. Yamada, S. General Shear-Thinning Dynamics of Confined Fluids. *Tribol. Lett.* **2002**, *13*, 167-171.
41. Yamada, S.; Nakamura, G.; Hanada, Y.; Amiya, T. Glasslike Transitions in Thin Polymer-Melt Films Due to Thickness Constraint. *Tribol. Lett.* **2003**, *13*, 83-89.
42. Ferry, J. D. *Viscoelastic Properties of Polymers*, 3<sup>rd</sup> Ed.; Wiley: New York, USA, 1980.
43. Luengo, G.; Israelachvili, J.; Dhinojwala, A.; Granick, S. Generalized Effects in Confined Fluids: New Friction Map for Boundary Lubrication. *Wear* **1996**, *200*, 328-335.
44. Utz, M.; Debenedetti, P.G.; Stillinger, F.H. Atomistic Simulation of Aging and Rejuvenation in Glasses. *Phys. Rev. Lett.* **2000**, *84*, 1471-1474.
45. Rottler, R.; Robbins, M.O. Unified Description of Aging and Rate Effects in Yield of Glassy Solids. *Phys. Rev. Lett.* **2005**, *95*, 225504.
46. Rottler, R.; Robbins, M.O. Macroscopic Friction Laws and Shear Yielding of Glassy Solids. *Comput. Phys. Commun.* **2005**, *169*, 177-182.
47. Ruina, A. Slip Instability and State Variable Friction Laws. *J. Geophys. Res.* **1983**, *88*, 10359-10370.

48. Berthoud, P.; Baumberger, T.; G'Sell, C.; Hiver, J.-M. Physical Analysis of the State- and Rate-Dependent Friction Law: Static Friction. *Phys. Rev. B* **1999**, *59*, 14313-14327.
49. Baumberger, T.; Caroli, C. Solid Friction from Stick-Slip down to Pinning and Aging. *Advance in Phys.* **2006**, *55*, 279-348.
50. Charrault, E.; Gauthier, C.; Marie, P.; Schirrer, R. Structural Recovery (Physical Ageing) of the Friction Coefficient of Polymers. *J. Polymer Sci. B Polymer Phys.* **2008**, *46*, 1337-1347.
51. The mechanical time constant of the experimental system is the order of milliseconds.
52. Sperling, L.H. *Introduction to Physical Polymer Science*, 3<sup>rd</sup> Ed.; Wiley Interscience: New York, USA, 2001.
53. Dowson, D. *History of Tribology*; Longman: London and New York, 1979.
54. Yoshizawa, H.; Chen, Y.L.; Israelachvili, J. Fundamental Mechanisms of Interfacial Friction. 1. Relation between Adhesion and Friction. *J. Phys. Chem.* **1993**, *97*, 4128-4140.
55. Yamada, S.; Nakamura, G.; Amiya, T. Shear Properties for Thin Films of Star and Linear Polymer Melts. *Langmuir* **2001**, *17*, 1693-1699.
56. Israelachvili, J. Tribology of Ideal and Non-Ideal Surfaces and Fluids. In *Fundamental of Tribology and Bridging the Gap between the Macro- and Micro/Nanoscales*; Bhushan, B., Ed.; Kluwer Academic Publishers: Dordrecht, The Netherlands, 2001; p. 631.
57. Berman, A.D.; Israelachvili, J.N. Control and minimization of friction via surface modification. In *Micro/Nanotribology and its Applications, NATO Advanced Science Institute Series*; Bhushan, B., Ed.; Kluwer Academic Publishers: Dordrecht, The Netherlands, 1997; p. 317.
58. Yoshizawa, H.; McGuiggan, P.; Israelachvili, J. Identification of a Second Dynamic State During Stick-Slip Motion. *Science* **1993**, *259*, 1305-1308.
59. Urbakh, M.; Klafter, J.; Gourdon, D.; Israelachvili, J. The Nonlinear Nature of Friction. *Nature* **2004**, *430*, 525-528.
60. Berman, A.D.; Ducker, W.A.; Israelachvili, J.N. Origin and characterization of different stick-slip friction mechanisms. *Langmuir* **1996**, *12*, 4559-4563.
61. Strictly speaking, the lateral velocity at the interface is not exactly zero but mechanical creep at a molecular level is expected [19,43]. This should be of course also expected for the case of stop-start stiction dynamics. This creep deformation is included in Figure 13a.
62. Israelachvili, J.N. Adhesion, Friction and Lubrication of Molecularly Smooth Surfaces. In *Fundamentals of Friction*; Singer, I.L., Pollock, H.M., Eds.; Kluwer Academic Publishers: Dordrecht, The Netherlands, 1992; p. 351.
63. Thompson, P.A.; Robbins, M.O. Origin of Stick-Slip Motion in Boundary Lubrication. *Science* **1990**, *250*, 792-794.
64. Akbulut, M.; Chen, N.; Maeda, N.; Israelachvili, J.; Grunewald, T.; Helm, C.A. Crystallization in Thin Liquid Films Induced by Shear. *J. Phys. Chem. B* **2005**, *109*, 12509-12514.
65. Richetti, P.; Drummond, C.; Israelachvili, J.; In, M.; Zana, R. Inverted Stick-Slip Friction. *Europhys. Lett.* **2001**, *55*, 653-659.
66. Drummond, C.; Elezgaray, J.; Richetti, P. Behavior of Adhesive Boundary Lubricated Surfaces under Shear: A New Dynamic Transition. *Europhys. Lett.* **2002**, *58*, 503-509.
67. Drummond, C.; Israelachvili, J.; Richetti, P. Friction between Two Weakly Adhering Boundary Lubricated Surfaces in Water. *Phys. Rev. E* **2003**, *67*, 066110.

68. Fillippov, A.E.; Klafter, J.; Urbakh, M. Inverted Stick-Slip Friction: What is the Mechanism? *J. Chem. Phys.* **2002**, *116*, 6871-6874.
69. Qian, L.-M.; Luengo, G.; Perez, E. Thermally Activated Lubrication with Alkanes: The Effect of Chain Length. *Europhys. Lett.* **2003**, *61*, 268-274.
70. Yamada, S. Nanotribology of Poly(dimethylsiloxane) Melt Confined between Hydrophobic Surfaces. *Tribol. Online* **2006**, *1*, 29-33.
71. Demirel, A.L.; Granick, S. Friction Fluctuation and Friction Memory in Stick-Slip Motion. *Phys. Rev. Lett.* **1996**, *77*, 4330-4333.
72. Demirel, A.L.; Granick, S. Origins of Solidification When a Simple Molecular Fluid is Confined between Two Plates. *J. Chem. Phys.* **2001**, *115*, 1498-1512.
73. Bureau, L. Rate Effects on Layering of a Confined Linear Alkane. *Phys. Rev. Lett.* **2007**, *99*, 225503.
74. Mukhopadhyay, A.; Zhao, J.; Bae, S.C.; Granick, S. Contrasting Diffusion and Viscosity in Molecularly-Thin Films. *Phys. Rev. Lett.* **2002**, *89*, 136103.
75. Heuberger, M. The Extended Surface Forces Apparatus. Part I. Fast Spectral Correlation Interferometry. *Rev. Sci. Instr.* **2001**, *72*, 1700-1707.
76. Dushkin, C.D.; Kurihara, K. Nanotribology of Thin Liquid-Crystal Films Studied by the Shear Force Resonance Method. *Colloids Surfaces A: Physicochem. Eng.* **1997**, *129-130*, 131-139.
77. Sakuma, H.; Otsuki, K.; Kurihara, K. Viscosity and Lubricity of Aqueous NaCl Solution Confined between Mica Surfaces Studied by Shear Resonance Measurement. *Phys. Rev. Lett.* **2006**, *96*, 046104.
78. Idziak, S.H.J.; Safinya, C.R.; Hill, R.; Kraiser, K.E.; Ruths, M.; Warriner, H.E.; Steinberg, S.; Liang, K.S.; Israelachvili, J.N. The X-Ray Surface Forces Apparatus: Structure of a Smectic Liquid Crystal under Confinement and Flow. *Science* **1994**, *264*, 1915-1918.
79. Mukhopadhyay, A.; Bae, S.C.; Zhao, J.; Granick, S. How Confined Lubricants Diffuse during Shear. *Phys. Rev. Lett.* **2004**, *93*, 236105.
80. Bae, S.C.; Lee, H.; Lin, Z.; Granick, S. Chemical Imaging in a Surface Forces Apparatus: Confocal Raman Spectroscopy of Confined Poly(dimethylsiloxane). *Langmuir* **2005**, *21*, 5685-5688.
81. Bae, S.C.; Wong, J.S.; Kim, M.; Jiang, S.; Hong, L.; Granick, S. Using Light to Study Boundary Lubrication: Spectroscopic Study of Confined Fluids. *Phil. Trans. R. Soc. A* **2008**, *366*, 1443-1454.
82. Jiang, S.; Bae, S.C.; Granick, S. PDMS Melts on Mica Studied by Confocal Raman Scattering. *Langmuir* **2008**, *24*, 1489-1494.